

Critical scaling for dense granular flow between parallel plates near jamming

Michio Otsuki,^{1,*} Kenta Hayashi,¹ and Kiwamu Yoshii^{1,2}

¹*Graduate School of Engineering Science, Osaka University,
1-3 Machikaneyama, Toyonaka, Osaka, 560-8531, Japan*

²*Department of Physics, Nagoya University, Furo-cho, Chikusa-ku, Nagoya, Aichi, 464-8602, Japan*
(Dated: March 4, 2024)

We numerically study the flow of dense granular materials between parallel plates driven by an external force. The granular materials form a jammed solid-like state when the external force is below a critical force, while they flow like fluids above the critical force. The transition is characterized by the mass flux. The critical force depends on the average packing fraction and the distance between the plates. The scaling laws for the critical force and the mass flux are predicted theoretically based on a continuum model. They are numerically verified.

I. INTRODUCTION

The dynamics of dense amorphous particles such as granular materials, suspensions, foams, and emulsions has been the subject of considerable investigation [1–3]. These materials can form a solid-like jammed state when the packing fraction ϕ exceeds a critical fraction ϕ_c , while they behave like fluids for $\phi < \phi_c$. Such a change in a rheological property is known as the jamming transition. The jammed particles above ϕ_c exhibit an elastic response under small shear stress σ , but they flow when σ exceeds the yield stress σ_Y [4]. In the vicinity of ϕ_c , the pressure, shear modulus, yield stress, and viscosity exhibit continuous transitions, which are characterized by critical power-law behavior [5–12]. In particular, it has been reported that the flow curve [13–18], complex shear modulus [19–21], relaxation modulus [22], mean square displacement [23, 24] obey critical scaling laws, similar to those for equilibrium critical phenomena.

Most previous studies of the jamming transition have focused on the critical behavior in homogeneous systems characterized by a constant packing fraction ϕ and shear rate $\dot{\gamma}$. However, in many manufacturing processes of dense amorphous particles, including granular materials, the formation of a solid-like jammed state is observed in inhomogeneous systems [25]. This phenomenon manifests in various forms, including clogging [26, 27], avalanches [28–31], and the separation of fluidized surface layers and frozen bulk regions [32–38]. Critical behavior is expected for jamming in these inhomogeneous systems. However, little is known about the critical behavior in inhomogeneous systems.

To analyze inhomogeneous granular flows, a continuum theory based on the $\mu(I)$ -rheology is useful [25]. In the $\mu(I)$ -rheology, a local constitutive equation is assumed, where the bulk friction

$$\mu = |\sigma|/p \quad (1)$$

with the shear stress σ and the normal pressure p is de-

scribed as a function of the inertia number:

$$I = \dot{\gamma}d/\sqrt{p/\rho_s}, \quad (2)$$

where $\dot{\gamma}$ is the shear rate, ρ_s is the solid grain density, and d is the mean particle diameter [25, 39–44]. Recent studies have improved the $\mu(I)$ -rheology to account for the non-local effect [44–50]. The $\mu(I)$ -rheology is known to reproduce the velocity profiles of various granular flows [31, 34, 38, 51, 52]. Therefore, we use it to analyze the critical behavior of the inhomogeneous flow in the vicinity of jamming.

In this paper, we numerically study the inhomogeneous steady flow of granular materials driven by an external force between parallel rough plates with the mean packing fraction ϕ_0 . In Sec. II, we explain the setup of our model. Section III deals with the numerical results of the granular flow. In Sec. IV, we analytically and numerically investigate scaling laws. The details of the continuum model are presented in Sec. IV A. In Sec. IV B, the scaling law of the critical force is derived. In Sec. IV C, the critical behavior of the mass flux is studied. We discuss and conclude our results in Sec. V. In Appendix A, we present the numerical results on the pressure and estimate the critical fraction. The details of the derivation of the scaling laws are presented in Appendix B.

II. SETUP

We consider two-dimensional granular materials consisting of N frictionless particles with identical density ρ_s between two parallel rough plates with the mean packing fraction ϕ_0 as shown in Fig. 1. The plates with length L along the x -direction are placed at $z = \pm H/2$ with distance H . We impose periodic boundary conditions in the x -direction. The particles are driven by an external force along the x -direction.

The equation of motion is given by

$$m_i \frac{d^2}{dt^2} \mathbf{r}_i = \sum_{j \neq i} \mathbf{F}_{ij} + m_i \mathbf{f} \mathbf{e}_x, \quad (3)$$

where m_i and $\mathbf{r}_i = (x_i, z_i)$ are the mass and position of particle i , respectively. Here, \mathbf{f} is the external force per

* m.otsuki.es@osaka-u.ac.jp

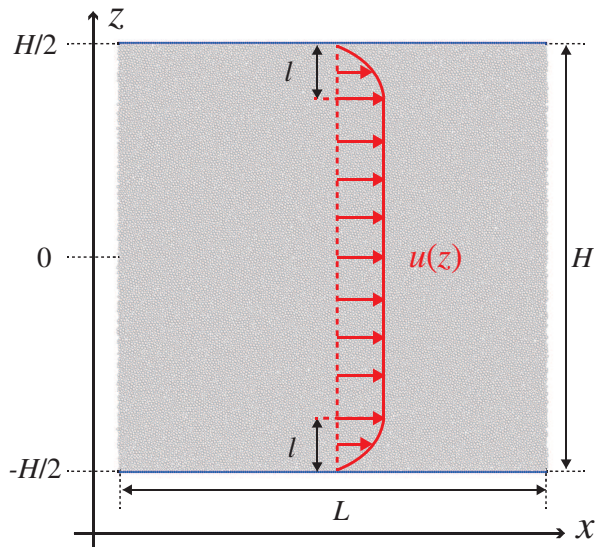


FIG. 1. Schematic of granular flows between rough parallel plates. Red line indicates schematic velocity profiles. Blue particles represent the rough plates. The size of the fluidized regions are represented by ℓ .

unit mass, and $\mathbf{e}_x = (1, 0)$ is the unit vector along the x -direction. The interaction force is given by

$$\mathbf{F}_{ij} = - \left(k u_{ij}^{(n)} + \eta v_{ij}^{(n)} \right) \Theta(d_{ij} - r_{ij}) \mathbf{n}_{ij}, \quad (4)$$

where $\Theta(x)$ is the Heaviside step function satisfying $\Theta(x) = 1$ for $x \geq 0$ and $\Theta(x) = 0$ for otherwise. The elastic constant, viscosity, and diameter of particle i are denoted by k , η , and d_i , respectively. Here, the relative displacement, the normal relative velocity, and the normal vector are given by $u_{ij}^{(n)} = r_{ij} - d_{ij}$, $v_{ij}^{(n)} = \frac{d}{dt} u_{ij}^{(n)}$, and $\mathbf{n}_{ij} = \mathbf{r}_{ij}/r_{ij}$, with $d_{ij} = (d_i + d_j)/2$, $\mathbf{r}_{ij} = \mathbf{r}_i - \mathbf{r}_j$, and $r_{ij} = |\mathbf{r}_{ij}|$, respectively.

The granular materials consist of an equal number of particles with diameters d_0 and $s d_0$, where s is the size ratio of two types of particles. The mean diameter is given by $d = (1 + s)d_0/2$. The mean packing fraction of this system is given by $\phi_0 = \pi N(1 + s^2)d_0^2/(8LH)$. The rough plates consist of particles with diameter d_0 placed at $(x, z) = (nd_0, \pm H/2)$ with an integer n . We first apply an external force large enough to generate flow, and the external force is changed to a given f . The steady parallel flow is realized after a sufficiently long relaxation time, as shown in Fig. 1. Particles in a long vertical pipe connected to a hopper [52] and those between pressure-controlled parallel walls [45, 51] exhibit similar parallel flows.

We use $L = 200d_0$, $s = 1.4$, and $\eta/\sqrt{m_0 k} = 1$, where m_0 is the mass of a particle with diameter d_0 . The critical packing fraction is estimated as $\phi_c \simeq 0.843$ in Appendix A, below which the particles cannot form the jammed solid-like state. The parallel flow for $\phi_0 < \phi_c$ has been

studied in Refs. [52–54], but we focus on dense systems with $\phi_0 \geq \phi_c$. The time evolution equation is solved numerically using LAMMPS (the open source molecular dynamics program from Sandia National Laboratories) with the time step $\Delta t = 0.05\sqrt{m_0/k}$ [55, 56]. The units of the velocity, the external force, and the mass flux are $v_0 = d_0/\sqrt{m_0/k}$, $f_0 = k d_0/m_0$, and $Q_0 = \sqrt{m_0 k}$, respectively.

III. FLOW NEAR JAMMING

Figure 2 displays the velocity profile $u(z)$ for various values of f with $\phi_0 = 0.850$ and $H = 400d_0$. Here, $u(z)$ is obtained as the average of the particle velocity $v_{i,x} = \frac{d}{dt} x_i$ at z . The velocity profile is symmetric about $z = 0$, and $u(z) = 0$ at the rough plates ($z = \pm H/2$). For $f = 1.4 \times 10^{-6} f_0$ and $f = 1.3 \times 10^{-6} f_0$, a plug flow with a constant velocity is visible near $z = 0$. Near the plates, fluidized regions with nonzero shear rate are observed, where the velocity profile appears parabolic. For $f = 1.2 \times 10^{-6} f_0$ and $f = 1.0 \times 10^{-6} f_0$, the velocity $u(z)$ is zero in the entire system. This indicates that the particles are jammed for small f .

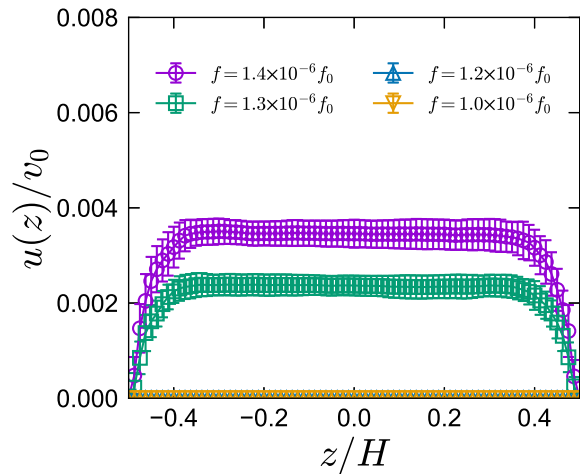


FIG. 2. Velocity profile $u(z)$ with $\phi_0 = 0.850$ and $H = 400d_0$ for various values of f .

In Fig. 3, the mass flux given by $Q = \sum_i m_i v_{i,x}/L$ is plotted against f for various values of ϕ_0 and H . The mass flux Q increases with H and decreases as ϕ_0 increases. For any ϕ_0 and H , Q increases from 0 as f exceeds a threshold f_c . The critical force f_c depending on ϕ_0 and H distinguishes the jammed state with $Q = 0$ from the unjammed state with $Q > 0$.

In Fig. 5, the critical force f_c is plotted against ϕ_0 for various values of H . We estimate f_c as the force f at which Q exceeds $Q_{th} = 1.0 \times 10^{-4} Q_0 (H/d_0)^2$. Note that f_c is unchanged if we choose a smaller Q_{th} . The critical force f_c increases as ϕ_0 exceeds $\phi_c \simeq 0.843$ and decreases as H increases. This indicates that the system jams as

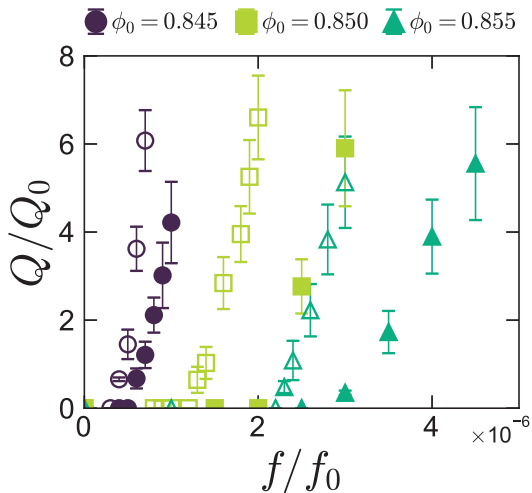


FIG. 3. Mass flux Q against f for various values of ϕ_0 with $H = 300d_0$ (filled symbols) and $H = 400d_0$ (open symbols).

H decreases or ϕ_0 increases.

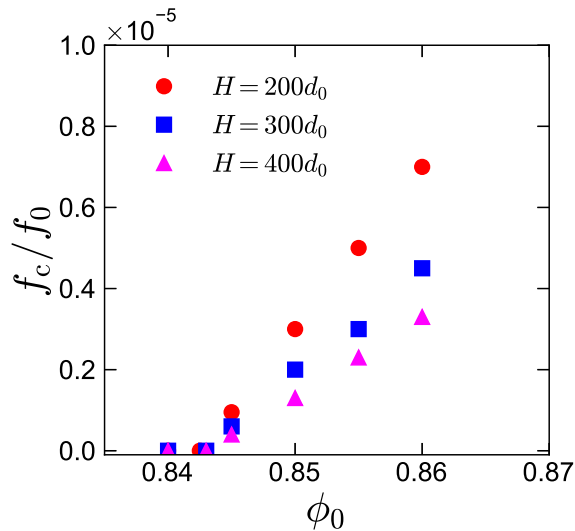


FIG. 4. Critical force f_c against ϕ_0 for various values of H .

IV. SCALING LAWS NEAR JAMMING

A. Continuum equations

In the steady flow shown in Fig. 2, the pressure $p(z)$, the shear stress $\sigma(z)$, and the packing fraction $\phi(z)$ at z

satisfy the momentum conservation [52, 57]

$$\frac{d\sigma(z)}{dz} = -\rho_s \phi(z) f, \quad (5)$$

$$\frac{dp(z)}{dz} = 0. \quad (6)$$

We adopt the $\mu(I)$ -rheology [25, 39] as the constitutive equation, where the local inertia number $I(z) = \dot{\gamma}(z)d/\sqrt{p(z)/\rho_s}$ and bulk friction coefficient $\mu(z) = |\sigma(z)|/p(z)$ satisfy

$$I(z) = \begin{cases} \mathcal{I}(\mu(z)) & (\mu(z) > \mu_s) \\ 0 & (\mu(z) \leq \mu_s), \end{cases} \quad (7)$$

with

$$\mathcal{I}(\mu) = I_0 \frac{\mu - \mu_s}{\mu_2 - \mu}, \quad (8)$$

and the shear rate $\dot{\gamma}(z) = |du(z)/dz|$. Here, μ_s is the static yield coefficient, μ_2 is the maximum value of μ , and I_0 is a dimensionless parameter characterizing the non-linear response. This constitutive equation indicates that the yield stress depends on the pressure, as $\sigma_Y = \mu_s p$. We assume that the local pressure $p(z)$ depends on the shear rate $\dot{\gamma}(z)$ and packing fraction $\phi(z)$: [10, 14–16, 58]

$$p(z) = \mathcal{P}(\dot{\gamma}(z), \phi(z)). \quad (9)$$

The function $\mathcal{P}(\dot{\gamma}, \phi)$ satisfies

$$\lim_{\dot{\gamma} \rightarrow 0} \mathcal{P}(\dot{\gamma}, \phi) = \Pi(\phi), \quad (10)$$

where $\Pi(\phi)$ is the pressure in the quasi-static limit, $\dot{\gamma} \rightarrow 0$. For particles with the linear repulsive interaction (Eq. (4)), $\Pi(\phi)$ obeys a scaling law [5]

$$\lim_{\phi \rightarrow \phi_c} \Pi(\phi) = B|\phi - \phi_c| \quad (11)$$

for $\phi \geq \phi_c$ with a constant B , which is numerically confirmed in our system as shown in Appendix A. Here, we have assumed that $\sigma(z)$ and $p(z)$ are determined by the local quantities $\dot{\gamma}(z)$ and $\phi(z)$, as the non-local effect is irrelevant for sufficiently large systems [45]. In fact, we have verified that the same analytical results are obtained for $H/d \gg 1$ even when we apply the non-local constitutive equation used in Ref. [45]. We have also verified that different forms of $\mathcal{I}(\mu)$ proposed in Refs. [40–44] give identical scaling laws for f_c and Q shown below.

The mean packing fraction ϕ_0 satisfies

$$\phi_0 = \int_{-H/2}^{H/2} dz \phi(z)/H. \quad (12)$$

The boundary condition is given by

$$u(z = \pm H/2) = 0. \quad (13)$$

The system is symmetric with respect to $z = 0$:

$$u(z) = u(-z), \quad (14)$$

$$\sigma(z) = -\sigma(-z). \quad (15)$$

The mass flux Q is given by

$$Q = \int_{-H/2}^{H/2} dz \rho_s \phi(z) u(z). \quad (16)$$

B. Critical force

First, we consider the jammed state with $\dot{\gamma}(z) = 0$ for $f < f_c$. From Eqs. (6), (9), (10), and (12) with $\dot{\gamma}(z) = 0$, $\phi(z)$ and $p(z)$ are given by

$$\phi(z) = \phi_0, \quad (17)$$

$$p(z) = \Pi(\phi_0), \quad (18)$$

respectively. Substituting Eq. (17) into Eq. (5) and using Eq. (15), we obtain

$$\sigma(z) = -\rho_s \phi_0 f z. \quad (19)$$

From Eqs. (18) and (19), the bulk friction $\mu(z) = |\sigma(z)|/p(z)$ is given by

$$\mu(z) = \rho_s \phi_0 f |z| / \Pi(\phi_0). \quad (20)$$

According to the constitutive equation, Eq. (7), the jammed state with $\dot{\gamma}(z) = 0$ is realized when $\mu(z) \leq \mu_s$ is satisfied for $-H/2 \leq z \leq H/2$. Using Eq. (20), this condition is replaced with $f \leq f_c$, where

$$f_c = \frac{2\mu_s \Pi(\phi_0)}{\rho_s \phi_0 H}. \quad (21)$$

For $\phi_0 - \phi_c \ll 1$, Eqs. (11) and (21) give the scaling law

$$f_c H = (f_0 d_0) \mathcal{F}(\phi_0 - \phi_c), \quad (22)$$

where $\mathcal{F}(\xi)$ denotes a scaling function. In our model, $\mathcal{F}(\xi)$ is given by $\mathcal{F}(\xi) = 2\mu_s B \xi / (\rho_s f_0 \phi_c d_0)$. In Fig. 5, we present the scaling plot based on Eq. (22), which demonstrates the collapse of all data points across various values of ϕ_0 and H . This consolidation confirms the validity of the scaling law expressed in Eq. (22). where the all the data with various ϕ_0 and H are nicely collapsed. This confirms the validity of the scaling law, Eq. (22).

C. Mass flux

Next, we focus on the critical behavior of the mass flux Q near f_c . By introducing a reduced force

$$\epsilon = \frac{f - f_c}{f_c}, \quad (23)$$

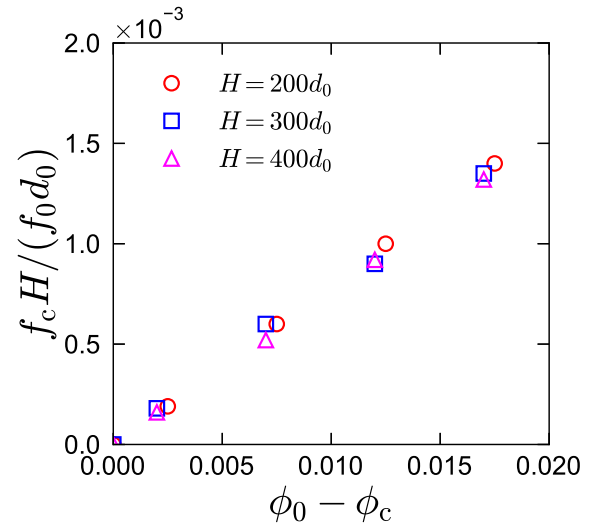


FIG. 5. Scaled plot of f_c based on Eq. (22) for various values of H .

we perturbatively obtain $\phi(z)$, $u(z)$, and Q for $\epsilon \ll 1$ from Eqs. (5)–(15). The details of the perturbation theory are shown in Appendix B. In the lowest order approximation, $\phi(z)$ and $p(z)$ are the same as the solutions for $\dot{\gamma} = 0$ given by Eqs. (17) and (18). The local shear rate $\dot{\gamma}(z)$ is given by

$$\dot{\gamma}(z) = \begin{cases} \frac{\mu_s I_0 \sqrt{\Pi(\phi_0)/\rho_s}}{(\mu_s - \mu_2)d} \epsilon \zeta(z) & (|z| > H/2 - \ell) \\ 0 & (|z| \leq H/2 - \ell), \end{cases} \quad (24)$$

with $\zeta(z) = (|z| - H/2 + \ell)/\ell$. The area for $|z| > H/2 - \ell$ represents the fluidized region with size ℓ as shown in Fig. 1, and $\zeta(z)$ represents the normalized position in the fluidized region. Size ℓ of the fluidized region is given by $\ell = H\epsilon/2$ for $\epsilon \ll 1$. Integrating the shear rate $\dot{\gamma}(z)$ with respect to z and using the boundary condition, Eq. (13), we obtain the velocity profile for $\epsilon \ll 1$ as

$$u(z) = \begin{cases} U_M |1 - \{\zeta(z)\}^2| & (|z| > H/2 - \ell) \\ U_M & (|z| \leq H/2 - \ell), \end{cases} \quad (25)$$

with the maximum velocity

$$U_M = \frac{\mu_s I_0}{4(\mu_s - \mu_2)} \frac{\sqrt{\Pi(\phi_0)/\rho_s} H}{d} \epsilon^2. \quad (26)$$

In the fluidized region for $|z| > H/2 - \ell$, the granular materials exhibit a parabolic velocity profile, while a plug flow appears for $|z| \leq H/2 - \ell$. This velocity profile is similar to that in yield stress fluids [59–61]. The velocity profile given by Eq. (25) is consistent with that in Fig. 2. A similar plug flow is obtained for granular materials with $\phi_0 < \phi_c$, but the critical force does not exist in relatively dilute systems [52–54].

The mass flux Q is obtained by substituting the solutions of $\phi(z)$ and $u(z)$ into Eq. (16) as

$$Q = \rho_s \phi_0 H U_M \quad (27)$$

for $\epsilon \ll 1$. Substituting Eqs. (11), (21), (23), and (26) into this equation, we obtain a critical scaling law near ϕ_c for the mass flux Q as

$$\frac{Q}{H^2 \sqrt{\phi_0 - \phi_c}} = (Q_0/d_0^2) \mathcal{Q} \left(\frac{fH/(f_0 d_0)}{\phi_0 - \phi_c} \right), \quad (28)$$

with a scaling function $\mathcal{Q}(\xi)$. In our analytical model, $\mathcal{Q}(\xi)$ is given by $\mathcal{Q}(\xi) = \alpha(\beta\xi - 1)^2$, with $\alpha = \frac{\mu_s I_0 \phi_0 \sqrt{\rho_s B} d_0^2}{4(\mu_s - \mu_2) d Q_0}$ and $\beta = \frac{\rho_s \phi_0 f_0 d_0}{2\mu_s B}$.

In Fig. 6, we demonstrate the scaling plot of the mass flux Q based on Eq. (28). Although the system is inhomogeneous, with the shear rate depending on z as shown in Fig. 2, we find excellent consolidation of data in Fig. 6, which mirrors critical scaling laws observed in homogeneous systems near jamming [13–22, 24].

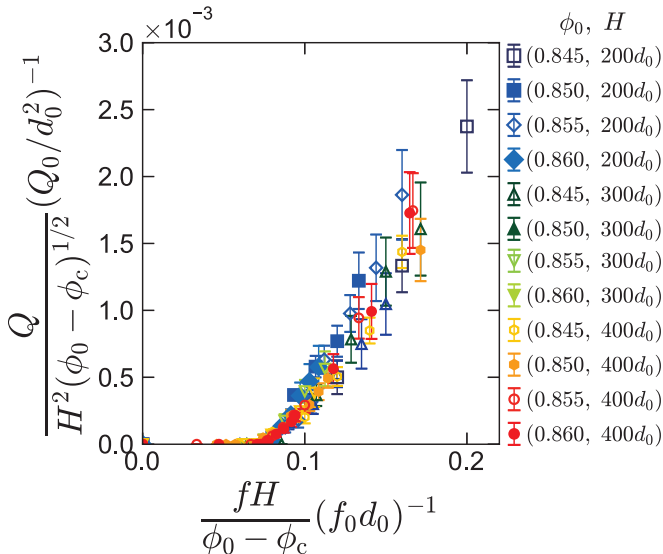


FIG. 6. Scaling plot of the mass flux Q based on Eq. (28) for various values of ϕ_0 and H . The legends represent (ϕ_0, H) .

V. CONCLUSION AND DISCUSSION

We have numerically studied the critical behavior of frictionless granular materials between rough parallel plates under an external force. Jamming is observed as the transition from the jammed state with the mass flux $Q = 0$ to the unjammed state with $Q > 0$ as f exceeds the critical force f_c . Based on a continuum model, we have analytically obtained the velocity profile $u(z)$, which gives the scaling laws for f_c and Q . The scaling laws have

been numerically verified. This indicates that critical behaviors similar to those in homogeneous systems can be observed in the inhomogeneous system.

In our analysis, we have considered the z -dependence of the packing fraction $\phi(z)$, but it is represented as a constant in the lowest order approximation. In previous studies based on continuum models [31, 34, 45, 51], the packing fraction is assumed as uniform, but we have confirmed that this assumption is justified for $\epsilon = (f - f_c)/f_c \ll 1$ with $\phi_0 \geq \phi_c$. For relatively dilute systems with $\phi_0 < \phi_c$, the critical force f_c is zero, and the z -dependence of the packing fraction $\phi(z)$ is essential [52–54].

We have considered frictionless particles with a repulsive interaction. However, we expect that critical behaviors are also observed in particles with friction or attractive interactions, as the $\mu(I)$ rheology is applicable in these systems [34, 62, 63]. An extension of our theory to these systems will be our future work.

ACKNOWLEDGMENTS

The authors thank R. Kuroda, K. Miyazaki, T. Uneyama, N. Oyama, H. Hayakawa, K. Saitoh, S. Takada, and T. Barker for fruitful discussions. M.O. is partially supported by JSPS KAKENHI (Grant Nos. JP21H01006 and JP23K03248). K.Y. is partially supported by JSPS Fellows (Grant No. 21J13720). K.Y. would like to thank the Research center for Computational Science, Okazaki, Japan for making its supercomputer system available (Project: 22-IMS-C267 and 23-IMS-C126). We would like to thank Editage (www.editage.jp) for English language editing.

The analytical calculation is performed by K.H and M.O. The numerical simulations using LAMMPS are performed by K.Y. The first draft of the manuscript was written by M.O.

Appendix A: Pressure in the jammed state

In this section, we present the numerical results for the pressure P , which is given by $P = \sum_i \sum_{j>i} (x_{ij} F_{ij,x} + y_{ij} F_{ij,y}) / (2LH)$ with $\mathbf{r}_{ij} = (x_{ij}, y_{ij})$ and $\mathbf{F}_{ij} = (F_{ij,x}, F_{ij,y})$. In Fig. 7, we plot the pressure P against $\phi_0 - \phi_c$ for $f = 0$. We estimate the critical packing fraction ϕ_c as ϕ_0 where P exceeds a threshold $P_{th} = 1.0 \times 10^{-5} f_0/d_0$ because the nonzero pressure is considered the indicator of jamming [5]. The critical fraction ϕ_c has a slight dependence on H as $\phi_c = 0.8425, 0.8430$, and 0.8430 for $H/d_0 = 200, 300$, and 400 , respectively. The pressure P is almost proportional to $\phi_0 - \phi_c$ in Fig. 7, which is consistent with Eq. (10).

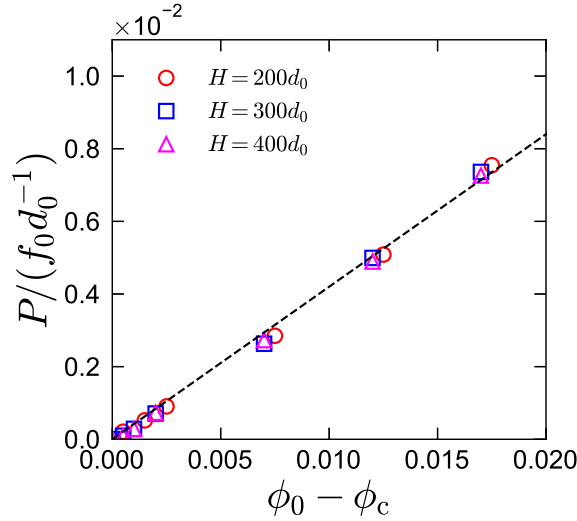


FIG. 7. Pressure P at the rough plates with $f = 0$ against $\phi_0 - \phi_c$ for various values of H . The dashed line represents Eq. (11) with $B = 0.4$.

Appendix B: Details of analysis

In this section, we demonstrate the details of our perturbation theory. From Eqs. (5) and (6) with Eq. (15), the stress and pressure are given by

$$\sigma(z) = -\rho_s f \int_0^z dz' \phi(z'), \quad (\text{B1})$$

$$p(z) = P_b, \quad (\text{B2})$$

where P_b is the pressure at the plates. Near $z = 0$, there is a region where $|\sigma|$ is less than $\mu_s P_b$. According to Eq. (7), the shear rate $\dot{\gamma}$ is zero in this region. The area for $|z| \leq H/2 - \ell$ corresponds to the plug region with $\dot{\gamma} = 0$, while the area for $|z| > H/2 - \ell$ represents the fluidized region with $\dot{\gamma} > 0$ with the size ℓ .

With the introduction of the nondimensionalized position

$$\zeta(z) = (|z| - H/2 + \ell)/\ell, \quad (\text{B3})$$

we represent the shear rate $\dot{\gamma}(z)$ as

$$\dot{\gamma}(z) = \begin{cases} \Gamma(\zeta(z)) & (|z| > H/2 - \ell) \\ 0 & (|z| \leq H/2 - \ell), \end{cases} \quad (\text{B4})$$

where $\Gamma(\zeta)$ is the shear rate in the fluidized region satisfying

$$\lim_{\zeta \rightarrow 0} \Gamma(\zeta) = 0. \quad (\text{B5})$$

According to Eqs. (9), (10), (B2), and (B4), the packing fraction $\phi(z)$ is constant in the plug region. Hence, $\phi(z)$

is represented as

$$\phi(z) = \begin{cases} \phi_s \{1 - \mathcal{F}(\zeta(z))\} & (|z| > H/2 - \ell) \\ \phi_s & (|z| \leq H/2 - \ell) \end{cases} \quad (\text{B6})$$

with the packing fraction ϕ_s in the plug region and a function $\mathcal{F}(\zeta)$ satisfying

$$\lim_{\zeta \rightarrow 0} \mathcal{F}(\zeta) = 0. \quad (\text{B7})$$

At the boundary of the plug region, $z = H/2 - \ell$, the shear stress σ satisfy $|\sigma| = \mu_s P_b$. Using Eqs. (B1), (B2), and (B6), this condition is replaced by

$$\mu_s P_b = \rho_s \phi_s f \left(\frac{H}{2} - \ell \right). \quad (\text{B8})$$

Substituting (B6) into Eq. (12), we obtain

$$\phi_0 = \phi_s \left\{ 1 - \frac{2\ell}{H} \int_0^1 d\zeta \mathcal{F}(\zeta) \right\}. \quad (\text{B9})$$

From Eqs. (B1), (B2), (B6), and (B8), we derive the bulk friction coefficient $\mu = |\sigma|/p$ at $\zeta \geq 0$ as

$$\mu(\zeta) - \mu_s = \mu_s \frac{\ell}{H/2 - \ell} \left\{ \zeta - \int_0^\zeta d\zeta' \mathcal{F}(\zeta') \right\}. \quad (\text{B10})$$

Substituting Eqs. (B2) and (B4) into Eq. (7) with $I = \dot{\gamma} d / \sqrt{p/\rho_s}$, we obtain

$$\frac{\Gamma(\zeta) d}{\sqrt{P_b/\rho_s}} = \mathcal{I}(\mu(\zeta) - \mu_s). \quad (\text{B11})$$

Using Eqs. (9) and (10) with Eqs. (B2), (B4), and (B6), we find

$$P_b = \Pi(\phi_s), \quad (\text{B12})$$

$$0 = \Delta(\phi_s \{1 - \mathcal{F}(\zeta)\}, \Gamma(\zeta)), \quad (\text{B13})$$

with $\Delta(\phi, \dot{\gamma}) = P(\phi, \dot{\gamma}) - \Pi(\phi)$, which satisfies $\lim_{\dot{\gamma} \rightarrow 0} \Delta(\phi, \dot{\gamma}) = 0$. From Eqs. (B8)-(B13), the variables ℓ , ϕ_s , P_b , $\Gamma(\zeta)$, and $\mathcal{F}(\zeta)$ are determined.

For $f \simeq f_c$ with $\epsilon \ll 1$, ℓ , ϕ_s , P_b , $\Gamma(\zeta)$, and $\mathcal{F}(\zeta)$ are expanded as

$$\ell = \epsilon \ell^{(1)} + O(\epsilon^2), \quad (\text{B14})$$

$$\phi_s = \phi_0 + \epsilon \phi_s^{(1)} + O(\epsilon^2), \quad (\text{B15})$$

$$P_b = \Pi(\phi_0) + \epsilon P_b^{(1)} + O(\epsilon^2), \quad (\text{B16})$$

$$\Gamma(\zeta) = \epsilon \Gamma^{(1)}(\zeta) + O(\epsilon^2), \quad (\text{B17})$$

$$\mathcal{F}(\zeta) = \epsilon \mathcal{F}^{(1)}(\zeta) + O(\epsilon^2). \quad (\text{B18})$$

Substituting these equations into Eqs. (B8)-(B13) and

extract all terms proportional to ϵ , we obtain

$$\ell^{(1)} = H/2, \quad (\text{B19})$$

$$\phi_S^{(1)} = 0, \quad (\text{B20})$$

$$P_b^{(1)} = 0, \quad (\text{B21})$$

$$\Gamma^{(1)}(\zeta) = \frac{\mu_s I_0 \sqrt{\Pi(\phi_0)/\rho_s}}{(\mu_2 - \mu_s)d} \zeta, \quad (\text{B22})$$

$$\mathcal{F}^{(1)}(\zeta) = \frac{C_1}{C_2 + C_3} \Gamma^{(1)}(\zeta), \quad (\text{B23})$$

with

$$C_1 = \left. \frac{\partial \Delta(\phi, \dot{\gamma})}{\partial \dot{\gamma}} \right|_{(\phi, \dot{\gamma})=(\phi_0, 0)}, \quad (\text{B24})$$

$$C_2 = \phi_0 \left. \frac{d\Pi(\phi)}{d\phi} \right|_{\phi=\phi_0}, \quad (\text{B25})$$

$$C_3 = \phi_0 \left. \frac{\partial \Delta(\phi, \dot{\gamma})}{\partial \phi} \right|_{(\phi, \dot{\gamma})=(\phi_0, 0)}. \quad (\text{B26})$$

Substituting these equations into Eqs. (B14)-(B18), we

obtain

$$\ell = \frac{H}{2}\epsilon + O(\epsilon^2), \quad (\text{B27})$$

$$\phi(z) = \phi_0 + O(\epsilon), \quad (\text{B28})$$

$$p(z) = \Pi(\phi_0) + O(\epsilon^2), \quad (\text{B29})$$

$$\dot{\gamma}(z) = \begin{cases} \frac{\mu_s I_0 \sqrt{\Pi(\phi_0)/\rho_s}}{(\mu_s - \mu_2)d} \epsilon \zeta(z) + O(\epsilon^2) & (|z| > H/2 - \ell) \\ 0 & (|z| \leq H/2 - \ell). \end{cases} \quad (\text{B30})$$

Neglecting the higher order terms in Eqs. (B27)-(B30), we obtain $\phi(z)$, $p(z)$, and $\dot{\gamma}(z)$ as Eqs. (17), (18), and (24), respectively.

Integrating $\dot{\gamma}(z)$ in Eq. (B30) with respect to z , we obtain

$$u(z) = \begin{cases} \tilde{U}_M \epsilon^2 |1 - \{\zeta(z)\}^2| + O(\epsilon^3) & (|z| > H/2 - \ell) \\ \tilde{U}_M \epsilon^2 + O(\epsilon^3) & (|z| \leq H/2 - \ell) \end{cases} \quad (\text{B31})$$

with

$$\tilde{U}_M = \frac{\mu_s I_0}{4(\mu_s - \mu_2)} \frac{\sqrt{\Pi(\phi_0)/\rho_s} H}{d}. \quad (\text{B32})$$

Neglecting $O(\epsilon^3)$ in Eq. (B31), we obtain Eq. (25). Substituting Eqs. (B28), (B31), and (B27) into Eq. (16), we obtain

$$Q = \rho_s \phi_0 \tilde{U}_M H \epsilon^2 + O(\epsilon^3). \quad (\text{B33})$$

Neglecting $O(\epsilon^3)$ in Eq. (B33), we obtain Eq. (27).

-
- [1] M. van Hecke, Jamming of soft particles: geometry, mechanics, scaling and isostaticity, *J. Phys. Condens. Matter* **22**, 033101 (2010).
- [2] R. P. Behringer and B. Chakraborty, The physics of jamming for granular materials: a review., *Rep. Prog. Phys.* **82**, 012601 (2019).
- [3] D. Bonn, M. M. Denn, L. Berthier, T. Divoux, and S. Manneville, Yield stress materials in soft condensed matter, *Rev. Mod. Phys.* **89**, 035005 (2017).
- [4] A. J. Liu and S. R. Nagel, Jamming is not just cool any more, *Nature* **396**, 21 (1998).
- [5] C. S. O'Hern, S. A. Langer, A. J. Liu, and S. R. Nagel, Random packings of frictionless particles, *Phys. Rev. Lett.* **88**, 075507 (2002).
- [6] C. S. O'Hern, L. E. Silbert, A. J. Liu, and S. R. Nagel, Jamming at zero temperature and zero applied stress: The epitome of disorder, *Phys. Rev. E* **68**, 011306 (2003).
- [7] M. Wyart, On the rigidity of amorphous solids, *Ann. Phys.* **30**, 1 (2005).
- [8] A. Zaccane and E. Scossa-Romano, Approximate analytical description of the nonaffine response of amorphous solids, *Phys. Rev. B* **83**, 184205 (2011).
- [9] M. Wyart, L. E. Silbert, S. R. Nagel, and T. A. Witten, Effects of compression on the vibrational modes of marginally jammed solids, *Phys. Rev. E* **72**, 051306 (2005).
- [10] T. Hatano, M. Otsuki, and S. ichi Sasa, Criticality and scaling relations in a sheared granular material, *J. Phys. Soc. Japan* **76**, 023001 (2007).
- [11] A. Ikeda, L. Berthier, and P. Sollich, Unified study of glass and jamming rheology in soft particle systems, *Phys. Rev. Lett.* **109**, 018301 (2012).
- [12] T. Kawasaki, D. Coslovich, A. Ikeda, and L. Berthier, Diverging viscosity and soft granular rheology in non-brownian suspensions, *Phys. Rev. E* **91**, 012203 (2015).
- [13] P. Olsson and S. Teitel, Critical scaling of shear viscosity at the jamming transition, *Phys. Rev. Lett.* **99**, 178001 (2007).
- [14] T. Hatano, Scaling properties of granular rheology near the jamming transition, *J. Phys. Soc. Japan* **77**, 123002 (2008).
- [15] M. Otsuki and H. Hayakawa, Universal scaling for the jamming transition, *Prog. Theor. Phys.* **121**, 647 (2009).
- [16] M. Otsuki and H. Hayakawa, Critical behaviors of

- sheared frictionless granular materials near the jamming transition, *Phys. Rev. E* **80**, 011308 (2009).
- [17] B. P. Tighe, E. Woldhuis, J. J. C. Remmers, W. van Saarloos, and M. van Hecke, Model for the scaling of stresses and fluctuations in flows near jamming, *Phys. Rev. Lett.* **105**, 088303 (2010).
- [18] K. N. Nordstrom, E. Verneuil, P. E. Arratia, A. Basu, Z. Zhang, A. G. Yodh, J. P. Gollub, and D. J. Durian, Microfluidic rheology of soft colloids above and below jamming, *Phys. Rev. Lett.* **105**, 175701 (2010).
- [19] B. P. Tighe, Relaxations and rheology near jamming, *Phys. Rev. Lett.* **107**, 158303 (2011).
- [20] M. Otsuki and H. Hayakawa, Avalanche contribution to shear modulus of granular materials, *Phys. Rev. E* **90**, 042202 (2014).
- [21] M. Otsuki and H. Hayakawa, Discontinuous change of shear modulus for frictional jammed granular materials, *Phys. Rev. E* **95**, 062902 (2017).
- [22] K. Saitoh and T. Kawasaki, Critical scaling of diffusion coefficients and size of rigid clusters of soft athermal particles under shear, *Front. Phys.* **8**, 99 (2020).
- [23] M. Otsuki and H. Hayakawa, Critical scaling of a jammed system after a quench of temperature, *Phys. Rev. E* **86**, 031505 (2012).
- [24] K. Saitoh, T. Hatano, A. Ikeda, and B. P. Tighe, Stress relaxation above and below the jamming transition, *Phys. Rev. Lett.* **124**, 118001 (2020).
- [25] G. D. R. MiDi, On dense granular flows, *Eur. Phys. J. E* **14**, 341 (2004).
- [26] I. Zuriguel, Invited review: Clogging of granular materials in bottlenecks, *Pap. Phys.* **6**, 060014 (2014).
- [27] G. Cai, A. B. Harada, and K. Nordstrom, Mesoscale metrics on approach to the clogging point, *Granul. Matter* **23**, 69 (2021).
- [28] O. Pouliquen, On the shape of granular fronts down rough inclined planes, *Phys. Fluids* **11**, 1956 (1999).
- [29] L. E. Silbert, J. W. Landry, and G. S. Grest, Granular flow down a rough inclined plane: Transition between thin and thick piles, *Phys. Fluids* **15**, 1 (2003).
- [30] Y. Forterre and O. Pouliquen, Stability analysis of rapid granular chute flows: formation of longitudinal vortices, *J. Fluid Mech.* **467**, 361 (2002).
- [31] D. Liu and D. L. Henann, Non-local continuum modelling of steady, dense granular heap flows, *J. Fluid Mech.* **831**, 212 (2017).
- [32] P.-A. Lemieux and D. J. Durian, From avalanches to fluid flow: A continuous picture of grain dynamics down a heap, *Phys. Rev. Lett.* **85**, 4273 (2000).
- [33] T. S. Komatsu, S. Inagaki, N. Nakagawa, and S. Nasuno, Creep motion in a granular pile exhibiting steady surface flow, *Phys. Rev. Lett.* **86**, 1757 (2001).
- [34] P. Jop, Y. Forterre, and O. Pouliquen, A constitutive law for dense granular flows, *Nature* **441**, 727 (2006).
- [35] D. Parker, A. Dijkstra, T. Martin, and J. Seville, Positron emission particle tracking studies of spherical particle motion in rotating drums, *Chem. Eng. Sci.* **52**, 2011 (1997).
- [36] F. Pignatelli, C. Asselin, L. Krieger, I. C. Christov, J. M. Ottino, and R. M. Lueptow, Parameters and scalings for dry and immersed granular flowing layers in rotating tumblers, *Phys. Rev. E* **86**, 011304 (2012).
- [37] A. V. Orpe and D. V. Khakhar, Scaling relations for granular flow in quasi-two-dimensional rotating cylinders, *Phys. Rev. E* **64**, 031302 (2001).
- [38] Q. Zheng, L. Bai, L. Yang, and A. Yu, 110th anniversary: continuum modeling of granular mixing in a rotating drum, *Ind. Eng. Chem.* **58**, 19251 (2019).
- [39] F. da Cruz, S. Emam, M. Prochnow, J.-N. Roux, and F. Chevoir, Rheophysics of dense granular materials: Discrete simulation of plane shear flows, *Phys. Rev. E* **72**, 021309 (2005).
- [40] T. Hatano, Power-law friction in closely packed granular materials, *Phys. Rev. E* **75**, 060301 (2007).
- [41] P.-E. Peyneau and J.-N. Roux, Frictionless bead packs have macroscopic friction, but no dilatancy, *Phys. Rev. E* **78**, 011307 (2008).
- [42] Émilien Azéma, F. Radjaï, and J.-N. Roux, Inertial shear flow of assemblies of frictionless polygons: Rheology and microstructure, *Eur. Phys. J. E* **41**, 2 (2018).
- [43] T. Man, P. Zhang, Z. Ge, S. A. Galindo-Torres, and K. M. Hill, Friction-dependent rheology of dry granular systems, *Acta Mech. Sin.* **39**, 722191 (2023).
- [44] M. Bouzid, M. Trulsson, P. Claudin, E. Clément, and B. Andreotti, Nonlocal rheology of granular flows across yield conditions, *Phys. Rev. Lett.* **111**, 238301 (2013).
- [45] K. Kamrin and G. Koval, Nonlocal constitutive relation for steady granular flow, *Phys. Rev. Lett.* **108**, 178301 (2012).
- [46] D. L. Henann and K. Kamrin, A predictive, size-dependent continuum model for dense granular flows, *Proc. Natl. Acad. Sci. U.S.A* **110**, 6730 (2013).
- [47] M. Bouzid, A. Izzet, M. Trulsson, E. Clément, P. Claudin, and B. Andreotti, Non-local rheology in dense granular flows, *Eur. Phys. J. E* **38**, 125 (2015).
- [48] Q. Zhang and K. Kamrin, Microscopic description of the granular fluidity field in nonlocal flow modeling, *Phys. Rev. Lett.* **118**, 058001 (2017).
- [49] S. Kim and K. Kamrin, Power-law scaling in granular rheology across flow geometries, *Phys. Rev. Lett.* **125**, 088002 (2020).
- [50] S. Kim and K. Kamrin, A second-order non-local model for granular flows, *Front. Phys.* **11**, 1092233 (2023).
- [51] D. Liu and D. L. Henann, Size-dependence of the flow threshold in dense granular materials, *Soft Matter* **14**, 5294 (2018).
- [52] T. Barker, C. Zhu, and J. Sun, Exact solutions for steady granular flow in vertical chutes and pipes, *J. Fluid Mech.* **930**, A21 (2022).
- [53] M. U. Islam, J. T. Jenkins, and S. L. Das, Extended kinetic theory for granular flow in a vertical chute, *J. Fluid Mech.* **950**, A13 (2022).
- [54] M. U. Islam, J. T. Jenkins, and S. L. Das, Granular flow through a vertical axisymmetric pipe, *Phys. Rev. Fluids* **8**, L072301 (2023).
- [55] S. Plimpton, Fast parallel algorithms for short-range molecular dynamics, *J. Comput. Phys.* **117**, 1 (1995).
- [56] A. P. Thompson, H. M. Aktulga, R. Berger, D. S. Bolintineanu, W. M. Brown, P. S. Crozier, P. J. in't Veld, A. Kohlmeyer, S. G. Moore, T. D. Nguyen, *et al.*, LAMMPS—a flexible simulation tool for particle-based materials modeling at the atomic, meso, and continuum scales, *Comput. Phys. Commun.* **271**, 108171 (2022).
- [57] D. J. Evans and G. Morriss, *Statistical Mechanics of Nonequilibrium Liquids* (Cambridge University Press, 2008).
- [58] K. Saitoh and H. Mizuno, Anomalous energy cascades in dense granular materials yielding under simple shear

- deformations, *Soft Matter* **12**, 1360 (2016).
- [59] J. G. Oldroyd, Two-dimensional plastic flow of a bingham solid, *Math. Proc. Camb. Philos. Soc.* **43**, 383 (1947).
- [60] I. A. Frigaard, S. D. Howison, and I. J. Sobey, On the stability of poiseuille flow of a bingham fluid, *J. Fluid Mech.* **263**, 133 (1994).
- [61] M. A. Khatib and S. Wilson, The development of poiseuille flow of a yield-stress fluid, *J. Fluid Mech.* **100**, 1 (2001).
- [62] T. T. Vo, S. Nezamabadi, P. Mutabaruka, J.-Y. Delenne, and F. Radjai, Additive rheology of complex granular flows, *Nat. Commun.* **11**, 1476 (2020).
- [63] S. Roy, S. Luding, and T. Weinhart, A general(ized) local rheology for wet granular materials, *New J. Phys.* **19**, 043014 (2017).